Reconstruction of Conductivity and Current Density Images Using Only One Component of Magnetic Field Measurements

Jin Keun Seo, Jeong-Rock Yoon, Eung Je Woo*, and Ohin Kwon

***Abstract*—Magnetic resonance current density imaging (MRCDI) is to provide current density images of a subject using a magnetic resonance imaging (MRI) scanner with a current injection apparatus. The injection current generates a magnetic field that we can measure from MR phase images. We obtain internal current density images from the measured magnetic flux densities via Ampere's law. However, we must rotate the subject to acquire all of the three components of the induced magnetic flux density. This subject rotation is impractical in clinical MRI scanners when the subject is a human body. In this paper, we propose a way to eliminate the requirement of subject rotation by careful mathematical analysis of the MRCDI problem. In our new MRCDI technique, we need to measure only one component of the induced magnetic flux density and reconstruct both cross-sectional conductivity and current density images without any subject rotation.**

***Index Terms*—Conductivity, current density, magnetic flux density, magnetic resonance current density imaging, magnetic resonance electrical impedance tomography.**

I. Introduction

Magnetic resonance current density imaging (MRCDI) has been developed to quantitatively visualize internal current density distributions of a subject due to an injection current through surface electrodes. The injection current generates a magnetic field and we measure the induced magnetic flux density within the subject using an magnetic resonance imaging (MRI) scanner. Then, we can obtain internal current density images from the measured magnetic flux densities via Ampere's law. This MRCDI technique has received considerable attention in medical imaging area last ten years following the pioneering works of Toronto group [1]–[5]. However, there still exist technical difficulties in its clinical applications due to two major limitations. One is the requirement of subject rotations within the MRI scanner. The other is the low signal-to-noise ratio (SNR) in magnetic flux density measurements. Lately, combining MRCDI and electrical impedance tomography (EIT) technique, magnetic resonance electrical impedance tomography (MREIT) has been suggested to provide cross-sectional conductivity or resistivity images of a subject [6]–[11]. In MREIT, we face the same limitations since it requires internal current density distributions obtained by the MRCDI technique. The purpose of this paper is to eliminate the problem related with subject rotations. If we do not have to rotate the subject, both current density and conductivity images in MRCDI and MREIT will find numerous clinical applications.

Manuscript received April 30, 2002; revised February 23, 2003. This work was supported by KOSEF under Grant R11-2002-103. The work of J. K. Seo was supported by the Korea Research Foundation under Grant 99-005-D0009. *Asterisk indicates corresponding author.*

J. K. Seo is with the Department of Mathematics, Yonsei University, Seoul 120-749, Korea.

J.-R. Yoon was with the School of Mathematics, Korea Institute for Advanced Study, Seoul 130-012, Korea. He is now with the Department of Mathematical Sciences, Rensselaer Polytechnic Institute, Troy, NY 12180-3590 USA.

*E. J. Woo is with the College of Electronics and Information, Kyung Hee University, 1 Seochun, Kiheung, Yongin, Kyungki, 449-701, S. Korea (e-mail: ejwoo@khu.ac.kr).

O. Kwon is with the Department of Mathematics, Konkuk University, Seoul 143-701, Korea.

Digital Object Identifier 10.1109/TBME.2003.816080

II. Mathematical Analysis: B_z-Based MRCDI Method

We place a subject inside an MRI scanner and inject a current I between two electrodes attached on its boundary. The injection current pulse is synchronized with a standard spin-echo pulse sequence as is usually done in the MRCDI technique [1]–[5]. The applied current I produces a current density $\mathbf{J} = (J_x, J_y, J_z)$ inside the subject. The presence of the internal current density $\mathbf{J}$ and the current I in lead wires generate a magnetic flux density $\mathbf{B} = (B_x, B_y, B_z)$. This induced magnetic flux density results in an incremental change in MR phase images that is proportional to B_z when z is the direction of the main magnetic field of the MRI scanner. We now assume that only B_z due to an injection current I is available without rotating the subject.

Since $\mu_0 \nabla \times \mathbf{J} = \nabla \times \nabla \times \mathbf{B} = -\nabla^2 \mathbf{B} + \nabla(\nabla \cdot \mathbf{B}) = -\nabla^2 \mathbf{B}$, we have

$$\begin{cases} -\frac{\partial J_y}{\partial x} + \frac{\partial J_x}{\partial y} = \frac{1}{\mu_0} \nabla^2 B_z \\ \mathbf{J} \cdot \mathbf{n} = g \end{cases} \tag{1}$$

where μ_0 is the magnetic permeability of the free space and biological tissues, $\mathbf{n}$ the outward unit normal vector, and g the normal component of current density on the boundary. Under an electrode E, we have $\int_E g\, ds = \pm I$ where the sign depends on the direction of current and g is zero on the regions of boundary not contacting with a current injection electrode. It is impossible to uniquely solve (1) since it has three unknowns $\mathbf{J} = (J_x, J_y, J_z)$.

We now set up two injection currents I^a and I^b so that the resulting current densities $\mathbf{J}^a = (J_x^a, J_y^a, J_z^a)$ and $\mathbf{J}^b = (J_x^b, J_y^b, J_z^b)$ satisfy

$$J_x^a J_y^b - J_y^a J_x^b \neq 0. \tag{2}$$

This implies that two current densities are not collinear inside the subject. Kim *et al.* rigorously proved that the condition in (2) can be satisfied for appropriately chosen I^a and I^b if the conductivity distribution σ satisfies a certain condition including $0 < \sigma < \infty$ (neither perfectly insulating nor perfectly conducting) [12].

We assume that σ is isotropic with $0 < \sigma < \infty$. Let u^a and u^b be the voltages due to injection currents I^a and I^b, respectively. Since σ is approximately independent of injection currents, each u^j ($j = a$ and b) is a solution of the following classical boundary value problem:

$$\begin{cases} \nabla \cdot (\sigma \nabla u^j) = 0 \\ \sigma \nabla u^j \cdot \mathbf{n} = -g^j. \end{cases} \tag{3}$$

The boundary value problem in (3) has a unique solution when we choose a ground or reference position with zero voltage. Hence, if σ and g^j are given, we can solve (3) using numerical methods such as the finite element method (FEM). Then, we can compute the corresponding current density as $\mathbf{J}^j = -\sigma \nabla u^j$.

In their early paper on MRCDI [1], Scott *et al.* already noted that $\nabla^2 \mathbf{B} = -\mu_0 \nabla u \times \nabla \sigma$. This enables us to rewrite (1) as

$$\begin{aligned} \frac{1}{\mu_0} \nabla^2 B_z^j &= -\frac{\partial J_y^j}{\partial x} + \frac{\partial J_x^j}{\partial y} \\ &= \left(\frac{\partial \sigma}{\partial x}, \frac{\partial \sigma}{\partial y} \right) \cdot \left(\frac{\partial u^j}{\partial y}, -\frac{\partial u^j}{\partial x} \right), \quad j = a \text{ and } b. \end{aligned} \tag{4}$$

Due to the choice of I^a and I^b with the condition in (2), we get

$$\begin{cases} \frac{\partial \sigma}{\partial x} = \frac{-\frac{\partial u^b}{\partial x} \nabla^2 B_z^a + \frac{\partial u^a}{\partial x} \nabla^2 B_z^b}{\mu_0 \left(-\frac{\partial u^a}{\partial y} \frac{\partial u^b}{\partial x} + \frac{\partial u^a}{\partial x} \frac{\partial u^b}{\partial y} \right)} \\ \frac{\partial \sigma}{\partial y} = \frac{-\frac{\partial u^b}{\partial y} \nabla^2 B_z^a + \frac{\partial u^a}{\partial y} \nabla^2 B_z^b}{\mu_0 \left(-\frac{\partial u^a}{\partial y} \frac{\partial u^b}{\partial x} + \frac{\partial u^a}{\partial x} \frac{\partial u^b}{\partial y} \right)}. \end{cases} \tag{5}$$

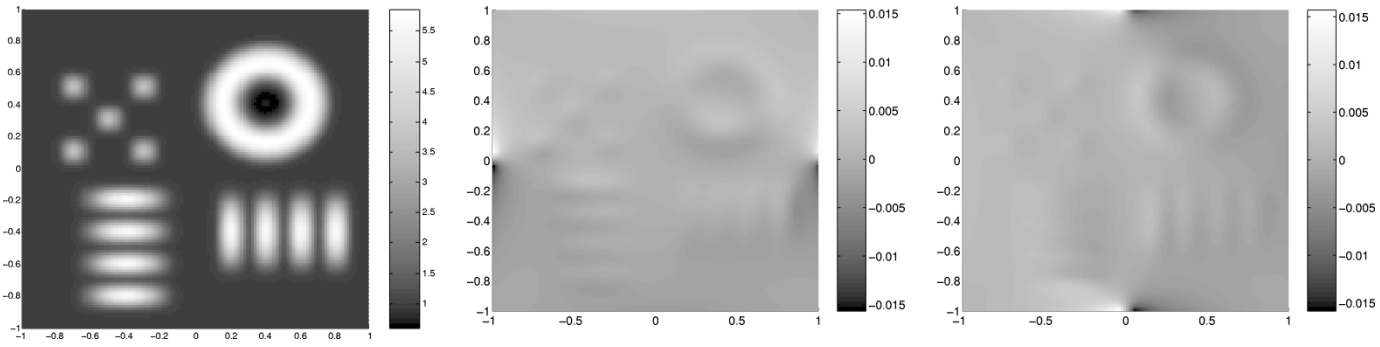

(a) (b) (c)

Fig. 1. (a) True conductivity distribution and simulated measured data for (b) B_z^a and (c) B_z^b.

Since we assume that σ is isotropic, we can express it in terms of u^j as

$$\sigma(x,y,z) = \sigma(x_0,y_0,z) + F\left[u^a,u^b\right](x,y,z) \tag{6}$$

where

$$F\left[u^a,u^b\right](x,y,z) = \int_{x_0}^{x}\left[\frac{\frac{\partial u^b}{\partial x}\nabla^2 B_z^a - \frac{\partial u^a}{\partial x}\nabla^2 B_z^b}{\mu_0\left(-\frac{\partial u^a}{\partial y}\frac{\partial u^b}{\partial x}+\frac{\partial u^a}{\partial x}\frac{\partial u^b}{\partial y}\right)}\right](t,y_0,z)\,dt + \int_{y_0}^{y}\left[\frac{\frac{\partial u^b}{\partial y}\nabla^2 B_z^a - \frac{\partial u^a}{\partial y}\nabla^2 B_z^b}{\mu_0\left(-\frac{\partial u^a}{\partial y}\frac{\partial u^b}{\partial x}+\frac{\partial u^a}{\partial x}\frac{\partial u^b}{\partial y}\right)}\right](x,t,z)\,dt.$$

Here, we assume that $\sigma(x_0,y_0,z)$ is known a priori. We will discuss how to handle this assumption later in this paper. It follows from (3) and (6) that u^a and u^b are solutions of the following system of nonlinear partial differential equations with $j = a$ and b:

$$\begin{cases}\nabla\cdot\left(\left(\sigma(x_0,y_0,z)+F\left[u^a,u^b\right]\right)\nabla u^j\right)=0\\ \left(\sigma(x_0,y_0,z)+F\left[u^a,u^b\right]\right)\nabla u^j\cdot\mathbf{n}=-g^j.\end{cases} \tag{7}$$

Hence, the reconstruction of conductivity and current density is reduced to solve (7) using the iterative algorithm described in Section III.

III. Reconstruction Algorithm: $\nabla^2 B_z$-Algorithm

We apply two currents I^a and I^b through electrodes placed on the boundary of a subject and measure z components of the induced magnetic flux densities, B_z^a and B_z^b. Then, our new algorithm is as follows.

Step 1) Assume an initial conductivity distribution σ_0. Compute $u_0^j (j = a$ and $b)$ by solving the boundary value problem in (3) with σ replaced by σ_0.

Step 2) For $m = 0,1,2,\cdots$, solve the following two Neumann boundary value problems for $j = a$ and b:

$$\begin{cases}\nabla\cdot\left(\left(\sigma(x_0,y_0,z)+F\left[u_m^a,u_m^b\right]\right)\nabla u_{m+1}^j\right)=0\\ \left(\sigma(x_0,y_0,z)+F\left[u_m^a,u_m^b\right]\right)\nabla u_{m+1}^j\cdot\mathbf{n}=-g^j.\end{cases} \tag{8}$$

Step 3) $\sigma = \lim_{m\to\infty}\sigma_m = \lim_{m\to\infty}(\sigma(x_0,y_0,z)+F[u_m^a,u_m^b])$.

Step 4) $\mathbf{J}^a \leftarrow -\sigma\nabla u^a$ and $\mathbf{J}^b \leftarrow -\sigma\nabla u^b$ where u^j is the solution of the boundary value problem in (3).

IV. Numerical Experiments

A. Preparation of Simulated Experimental Data

All numerical experiments are performed for the cubic subject $\mathcal{D} = (-1,1)\times(-1,1)\times(-1,1)$. We define an imaging slice of $\mathcal{D}_s = \{(x,y,s)|-1<x,y<1\}$ with a fixed value s in (−1,1) and discretize $\mathcal{D}_s$ into 128 × 128 pixels. In this section, we assume only for the simplicity of computations that σ does not change along z direction. Fig. 1(a) shows the true conductivity distribution used in numerical simulations. Let g^a and g^b be applied current densities given by

$$g^a = \begin{cases}-1, & \text{on } E_+^a\\ 1, & \text{on } E_-^a\\ 0, & \text{otherwise}\end{cases} \quad\text{and}\quad g^b = \begin{cases}-1, & \text{on } E_+^b\\ 1, & \text{on } E_-^b\\ 0, & \text{otherwise}\end{cases}$$

where $E_\pm^a = \{(\pm1,y,z) : |y|\le 0.05, |z|\le 1\}$ and $E_\pm^b = \{(x,\pm1,z) : |x|\le 0.05, |z|\le 1\}$. Given σ, g^a, and g^b, simulated data for voltage and current density distributions are numerically computed using FEM [13]. Next, we calculate magnetic flux densities B_z^a and B_z^b on three consecutive imaging slices of $\mathcal{D}_{-\delta}$, $\mathcal{D}_0$, and $\mathcal{D}_\delta$ using the Biot-Savart law. Fig. 1(b) and (c) shows B_z^a and B_z^b in $\mathcal{D}_0$, respectively.

Since we do not know the explicit geometry of lead wires, the magnetic flux densities in Fig. 1(b) and (c) could be different from the actual measured magnetic flux densities. However, any difference between measured and computed magnetic flux densities due to unknown lead wire geometry becomes irrelevant in our reconstruction algorithm by taking the Laplacian of them.

B. Image Reconstruction

With the homogeneous initial guess $(\sigma_0 = 1)$, the gradient of σ_m in the m-th iteration is calculated using (5) and the conductivity is updated with the relation in (6). Fig. 2(a) shows the reconstructed conductivity image in $\mathcal{D}_0$ after 10 iterations without added noise. Next, we added a random noise in B_z^j. The amount was 1% of the average value of $|B_z^j|$. Then, we applied the total variation based denoising technique [14] as was done in experimental study by Khang *et al.* [11]. Fig. 2(b) shows the reconstructed conductivity image in the same imaging slice after ten iterations.

Assuming that we inject a current of 10 mA into a subject with $200\times200\times200$ mm^3, we computed the average value of $|B_z^j|$ as 12.4 nT using the three-dimensional forward solver [13]. Based on the sensitivity analysis of MRCDI technique by Scott *et al.* [2], the noise standard deviation in the measured magnetic flux density could be about 0.75 nT which is 6% of the average value. Here, we assume that the SNR of MR magnitude image is 50 and the duration of current injection is 50 ms. Fig. 2(c) shows the reconstructed conductivity image with 6% added random noise after using the same denoising technique.

From the reconstructed conductivity image, we can obtain current density images from $\mathbf{J}^j = -\sigma\nabla u^j$. Fig. 3(a) shows the true current density image of $|\mathbf{J}^b|$. Fig. 3(b) shows the corresponding reconstructed current density image with its vector plot in Fig. 3(c) using the reconstructed conductivity in Fig. 2(a).

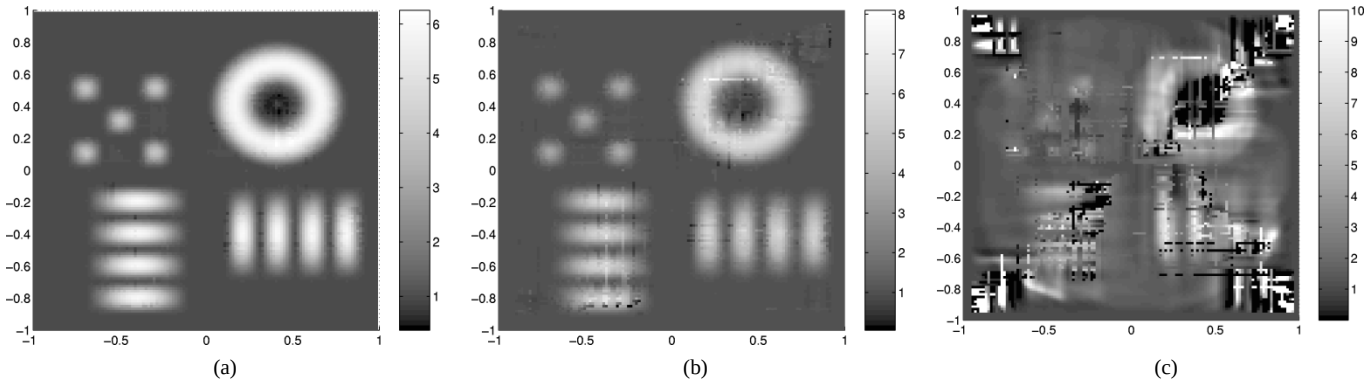

(a) (b) (c)

Fig. 2. Reconstructed conductivity images after ten iterations: (a) without added noise, (b) with 1% added noise, and (c) with 6% added noise.

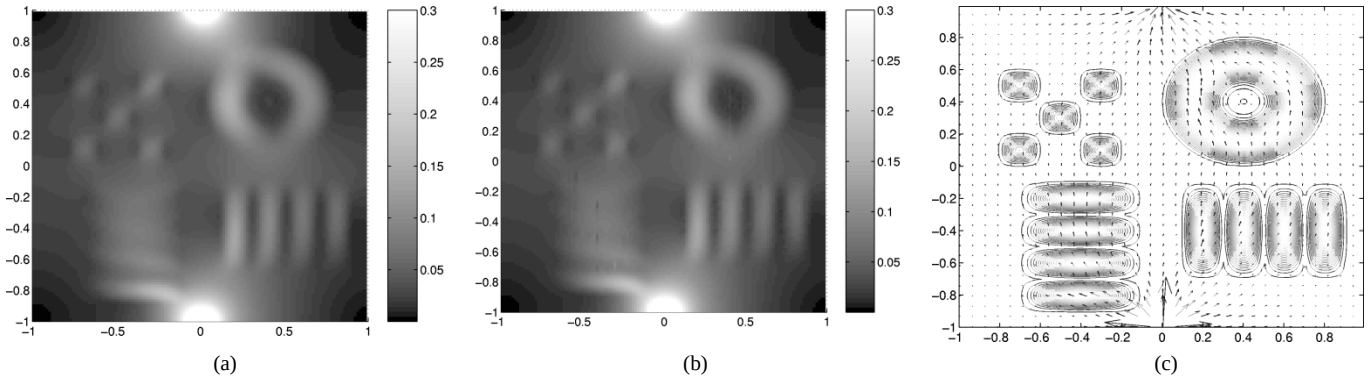

(a) (b) (c)

Fig. 3. (a) True current density image of $|\mathbf{J}^b|$. (b) Corresponding reconstructed current density image and (c) its vector plot.

V. Discussion

Our B_z-based MRCDI algorithm, which we call $\nabla^2 B_z$-algorithm, theoretically solves the subject rotation problem in conventional MRCDI techniques. The mathematical analysis and numerical simulation described in the previous sections show that the new method can provide both conductivity and current density images without subject rotation. However, there still are several things we must consider before we apply it to actual measured B_z data.

In our reconstruction algorithm, we must compute $\nabla^2 B_z$. These numerical differentiations are vulnerable to measurement noise. Practically, this is a very important problem since the SNR in magnetic flux density measurements is relatively low as shown in [2]. In addition to the considerations described by Scott *et al.* [2] including the voxel size and others, this requires us to use a very effective denoising technique. Using the total variation based denosing technique [14], we could reconstruct the conductivity image shown in Fig. 2(b) for the case of 1% added noise. This was possible since the true conductivity distribution was smooth so that B_z was also smooth being not affected much by the denoising procedure. However, as shown in Fig. 2(c), the reconstructed conductivity image is deteriorated when we add 6% random noise. Considering the more realistic situations where the amount of noise is larger than 6%, we must carefully study noise characteristics in measured B_z data and develop more effective denoising techniques based on underling physical principles. This will be one of our future research goals.

In numerical simulations, we assumed that the true conductivity distribution does not change along z direction for the simplicity of numerical computations. For a subject with an arbitrary σ, we may define a region of interest (ROI) that consists of several slices including electrodes. The length of the ROI is large enough so that the z components of current density at the top and bottom slice are negligibly small. This enables us to solve (8) in the ROI with $g = J_z = 0$ on the top and bottom slice. Then, our reconstruction procedure will require measured B_z data from multiple slices within the ROI. We need to further investigate the appropriate length of the ROI to compromise the quality of reconstructed image at the central slice with the required computation time.

As described earlier, it is necessary to know the conductivity value at one point on each imaging slice to obtain absolute values of conductivity distributions. This can be done by attaching a bar with a known conductivity value on the surface of the subject. Or, we presumably set the conductivity value on a fixed point to be one. We reconstruct the conductivity distribution following the procedure described in the previous section and obtain current density distributions. Then, we use the J-substitution algorithm in [10] with at least one boundary voltage measurement to reconstruct absolute values of the conductivity distribution.

The iterative algorithm described in this paper showed good convergence characteristics from simulations with a smooth conductivity distribution and a small amount of noise. However, we must work on a more rigorous mathematical proof on the convergence of the proposed algorithm. We do not assert that the algorithm described in this paper is optimal in reconstructing conductivity and current density images using B_z data with measurement noise. Rather, we would like to emphasize that the mathematical analysis on the new MRCDI technique proves the possibility of reconstructing conductivity and current density images without subject rotation. Our future study will include different reconstruction algorithms possessing robustness against measurement noise.

VI. Conclusion

MRCDI will be a valuable tool in many biomedical applications especially where we use electrical stimulation techniques. MREIT based

on MRCDI is also very promising to reconstruct cross-sectional conductivity images of a subject with improved spatial resolution and accuracy. However, both of them suffer from the requirement of subject rotations within an MRI scanner. In this paper, we described the mathematical analysis of a new MRCDI and MREIT technique without subject rotation. The new technique is based on measurements of only one component of the induced magnetic flux density. We also developed the image reconstruction algorithm for both conductivity and current density images.

Even though the mathematical analysis is complete and the reconstruction algorithms performs quite well for simulated B_z data with a smooth conductivity distribution and a small amount of noise, the performance of the algorithm could be significantly deteriorated when the SNR in B_z data is low. We are working on more effective denoising techniques and also different reconstruction algorithms with robustness against measurement noise. We also plan to do experimental works aiming to reconstruct 64×64 images with voxels of about $3 \times 3 \times 3\ \mathrm{mm}^3$.

REFERENCES

[1] G. C. Scott, M. L. G. Joy, R. L. Armstrong, and R. M. Henkelman, "Measurement of nonuniform current density by magnetic resonance," *IEEE Trans. Med. Imag.*, vol. 10, pp. 362–374, Sept. 1991.

[2] ——, "Sensitivity of magnetic-resonance current density imaging," *J. Magn. Reson.*, vol. 97, pp. 235–254, 1992.

[3] M. Eyuboglu, R. Reddy, and J. S. Leigh, "Imaging electrical current density using nuclear magnetic resonance," *Elektrik*, vol. 6, no. 3, pp. 201–214, 1998.

[4] H. R. Gamba, D. Bayford, and D. Holder, "Measurement of electrical current density distribution in a simple head phantom with magnetic resonance imaging," *Phys. Med. Biol.*, vol. 44, pp. 281–91, 1999.

[5] M. L. G. Joy, V. P. Lebedev, and J. S. Gati, "Imaging of current density and current pathways in rabbit brain during transcranial electrostimulation," *IEEE Trans. Biomed. Eng.*, vol. 46, pp. 1139–1149, Sept. 1999.

[6] N. Zhang, "Electrical Impedance Tomography based on Current Density Imaging," MS Thesis, Dept. Elect. Eng., Univ. bToronto, Toronto, ON, Canada, 1992.

[7] E. J. Woo, S. Y. Lee, and C. W. Mun, "Impedance tomography using internal current density distribution measured by nuclear magnetic resonance," *Proc. SPIE*, vol. 2299, pp. 377–385, 1994.

[8] Y. Z. Ider and O. Birgul, "Use of the magnetic field generated by the internal distribution of injected currents for Electrical Impedance Tomography (MR-EIT)," *Elektrik*, vol. 6, no. 3, pp. 215–225, 1998.

[9] M. Eyuboglu, O. Birgul, and Y. Z. Ider, "A dual modality system for high resolution-true conductivity imaging," in *Proc. XI Int. Conf. Electrical Bioimpedance (ICEBI)*, 2001, pp. 409–413.

[10] O. Kwon, E. Woo, J. Yoon, and J. K. Seo, "Magnetic resonance electrical impedance tomography (MREIT): Simulation study of J-substitution algorithm," *IEEE Trans. Biomed. Eng.*, vol. 49, pp. 160–167, Feb. 2002.

[11] H. S. Khang, B. I. Lee, S. H. Oh, E. J. Woo, S. Y. Lee, M. H. Cho, O. I. Kwon, J. R. Yoon, and J. K. Seo, "J-substitution algorithm in magnetic resonance electrical impedance tomography (MREIT): Phantom experiments for static resistivity images," *IEEE Trans. Med. Imag.*, vol. 21, pp. 695–702, June 2002.

[12] S. W. Kim, O. Kwon, J. K. Seo, and J. Yoon, "On a nonlinear partial differential equation arising in magnetic resonance electrical impedance tomography," *SIAM J. Math Anal.*, vol. 34, no. 3, pp. 511–526, 2002.

[13] B. I. Lee, S. H. Oh, E. J. Woo, S. Y. Lee, M. H. Cho, O. Kwon, J. R. Yoon, and J. K. Seo, "Three-dimensional forward problem in magnetic resonance electrical impedance tomography (MREIT)," in *Proc. 2nd Joint IEEE EMBS/BMES Conf.*, 2002, pp. 967–968.

[14] T. Chan, A. Marquina, and P. Mulet, "High-order total variation-based image restoration," *SIAM J. Sci. Comput.*, vol. 22, no. 2, pp. 503–516, 2000.

In Vivo Measurement of the Brain and Skull Resistivities Using an EIT-Based Method and the Combined Analysis of SEF/SEP Data

S. Gonçalves*, J. C. de Munck, J. P. A. Verbunt, R. M. Heethaar, and F. H. Lopes da Silva

***Abstract*—Results of *"in vivo"* measurements of the skull and brain resistivities are presented for six subjects. Results are obtained using two different methods, based on spherical head models. The first method uses the principles of electrical impedance tomography (EIT) to estimate the equivalent electrical resistivities of brain (ρ_{brain}), skull (ρ_{skull}) and skin (ρ_{skin}) according to [1]. The second one estimates the same parameters through a combined analysis of the evoked somatosensory cortical response, recorded simultaneously using magnetoencephalography (MEG) and electroencephalography (EEG).**

The EIT results, obtained with the same relative skull thickness (0.05) for all subjects, show a wide variation of the ratio $\rho_{\mathrm{skull}}/\rho_{\mathrm{brain}}$ among subjects (average $= 72$, SD $= 48\%$). However, the $\rho_{\mathrm{skull}}/\rho_{\mathrm{brain}}$ ratios of the individual subjects are well reproduced by combined analysis of somatosensory evoked fields (SEF) and somatosensory evoked potentials (SEP). These preliminary results suggest that the $\rho_{\mathrm{skull}}/\rho_{\mathrm{brain}}$ variations over subjects cannot be disregarded in the EEG inverse problem (IP) when a spherical model is used. The agreement between EIT and SEF/SEP points to the fact that whatever the source of variability, the proposed EIT-based method <Au: Addition of "method" O.K? appears to have the potential to reduce systematic errors in EEG IP associated to the misspecification of $\rho_{\mathrm{skull}}/\rho_{\mathrm{brain}}$, ρ_{brain}, ρ_{skull} and ρ_{skin}.

***Index Terms*—EEG inverse problem, electric impedance tomography, electrical resistivities, somatosensory evoked responses, three-layer sphere head model.**

I. INTRODUCTION

The importance of the "*in vivo*" measurement of the equivalent electric resistivities of brain, skull and scalp and their effect in improving the solution of the electroencephalography (EEG) inverse problem (IP) [2] has already been reported on a previous publication [1].

In principle, one could derive information about the individual's electrical resistivities by injecting currents and measuring the resulting potential distribution, i.e., using electrical impedance tomography [3] (EIT). In [4], this idea has been applied in practice on the real data of two subjects. Because of the isolating effect of the skull, a large part of the current will flow through the skin, and the amount of information that can be extracted from the potential measurements is limited. For that reason, it has to be assumed that the brain consists of compartments with known geometry and unknown resistivity. In [4], it was furthermore assumed that the resistivity of the skin and the brain are

Manuscript received September 13, 2001; revised February 23, 2003. The work of S. Gonçalves was supported by the Portuguese Foundation for Science and Technology under Ph.D. scholarship Praxis XXI/BD/15502/96. *Asterisk indicates corresponding author.*

*S. Gonalves is with the MEG Centre—Vrije Universiteit Medical Centre, Reception C, De Boelelaan 1117,1081 HV, Amsterdam, The Netherlands and also with the Institute of Biophysics and Biomedical Engineering, Faculty of Sciences, University of Lisbon, 1700 Campo Grande, Lisbon, Portugal (e-mail: s.goncalves@vumc.nl).

J. C. de Munck and J. P. A. Verbunt are with the MEG Centre—Vrije Universiteit Medical Centre, 1081 HV Amsterdam, The Netherlands.

R. M. Heethaar is with the Laboratory of Clinical Physics and Informatics, Institute of Cardiovascular Research ICaR-VU, University Hospital Vrije Universiteit, 1007 MB Amsterdam, The Netherlands.

F. H. L. da Silva is with the Institute of Neurobiology, 1098 SM Amsterdam, The Netherlands.

Digital Object Identifier 10.1109/TBME.2003.816072